Interlayer Torsional Sliding and Strain Localization in Bilayer Graphene

Qingxiang Ji[1], Zhiming Xue[1,2], Zaoxu Zhang[1], Zhanbo Cui[2], Muamer Kadic[3] and Changguo Wang[1]

[1]National Key Laboratory of Science and Technology on Advanced Composites in Special Environments, Harbin Institute of Technology, Harbin, 150001, China
[2]Technical Center, Haishan Corporation of Industrial Development in Shijiazhuang, Shijiazhuang, 050208, China
[3]Institute FEMTO-ST, CNRS, University Bourgogne Franche-Comté, Besançon 25000, France

Research

Article submitted to journal

Subject Areas:
Computational mechanics, Computational physics, Materials science

Keywords:
Twisted bilayer graphene; Van der Waals interaction; Torsional deformation; Strain localization

Author for correspondence:
Muamer Kadic, Changguo Wang
e-mail: muamer.kadic@femto-st.fr, wangcg@hit.edu.cn

Twisted bilayer graphene can demonstrate extraordinary optical and electrical characteristics due to its interlayer interactions. The strong coupling of normal and tangential van der Waals interactions at the interface results in inhomogeneous interlayer deformations and further changes the bilayer graphene's physical properties. Herein, theoretical and numerical models are established to study the torsional deformation behavior of twisting a graphene flake over a rigid graphene substrate. It is found that in-plane deformations have significant influences on the interlayer potential energy density of AA stacking, but seldom affect other stacked domains. The deformation process is thus approximated by first twisting the graphene flake rigidly, and then relaxing the rigid constraints. The bilayer graphene system minimizes its energy by reducing (enlarging) the size of high-energy (low-energy) domains through additional rotations. The additional angles of the graphene flake are derived analytically based on a mechanical model following the principle of minimum potential energy. Results show that the influences of graphene film deformations get significant at small-twist-angles (typically less than 2°). This work reveals the torsional deformation evolution mechanism of bilayer graphene and provides beneficial guidance on achieving intriguing physical properties.

1. Introduction

Graphene has recently drawn increasing attention for their extraordinary properties in hyper elasticity [1,2], piezoelectricity [3,4], frictional characteristics [5–7], optical properties [8–13] and so on. In particular, bilayer structures or van der Waals materials that feature more tunability in physical characteristics are formed by stacking graphene on top of one another. Twisted bilayer graphene (TBG) with a specific twist angle (magic-angle) can demonstrate intriguing properties, i.e., insulator characteristics, superconductivity and anomalous quantum hall effect [14–17]. Indeed, the twisting of graphene layers will lead to direction mismatch and result in a periodic Moiré pattern, which significantly changes electronic structures, transport, disorder and interactions of the TBG system [14,18]. Due to the unique structure of graphene lattices, the twist angle becomes a key controlled degree of freedom to regulate electronic and optical properties of TBGs [19,20]. It is important to fully understand the torsional behavior of TBGs with variance of the twist angle. In some ways, graphene posses many extraordinary properties like metamaterials which are an alternative way to stucture the matter at bigger scale with the quest of properties beyond those of the constituents [21–25]. Recently, elastic metamaterials took a similar direction based on quasi-crystals [26] and higher order interactions [27–29].

So far, researchers have mostly focused on TBG's rigid twisting behavior without considering any deformations. However, the interlayer van de Waals forces will inevitably result in both in-plane and out-of-plane deformations. These slight deformations can further change the electronic bands of the TBG system, i.e., the deformations require that the TBG reduces AA stacked domains and increases AB stacked domains. Alden et al. [30] found that AB stacking is the dominated manner in Moiré pattern. Zhang et al. [31] revealed local rotating and shrinking mechanism of the AA stacked domains in twisted graphene films: the local rotation angle is first invariant (then linear-correlated) with the interlayer twist angle, as the latter is within (beyond) the critical value. Kazmierczak et al. [32] experimentally demonstrated the nanoscale deformation of TBG and found that relative stacking order domains varied differently as the interlayer twist angle reached 0.5°.

Though the influences of deformations on TBG's physical properties are explored, the deformation evolution mechanism and strain characteristics still remain unclear. In this work we have studied the scaling law of interlayer potential energy density (IED) during the rigid twisting process. The deformation and strain characteristics of the graphene film is then presented considering released rigid constraints. We establish the strain potential energy function of deformed graphene films, and theoretically analyze the evolution mechanism of both in-plane and out-of-plane deformations following the principle of minimum potential energy. This work is of great significance in understanding the deformation mechanism of TBG and achieving more intriguing phenomenon.

2. Numerical study on torsional sliding of bilayer graphene

We have built a numerical model of TBG, where the graphene substrate is defined as a rigid that generates interlayer interaction without any deformation. In case of rigid twisting, Moiré pattern diameter λ, namely the distance between nearby AA stacked points, can be determined by [33]

$$\lambda = \frac{\sqrt{3}a}{2sin(\frac{\theta}{2})} \tag{2.1}$$

where θ is the twist angle and $a = 0.142$ nm denotes carbon-carbon bond length of the graphene lattices. It is observed from Fig. 1a that λ decreases first sharply and then slowly with the increment of θ, which indicates that the structural size should be large enough so that relative small twist angles can result in Moiré pattern. In addition, we define shell element size as 0.2 nm. A circular-shaped graphene model is employed to suppress the edge effects, and all degrees of freedom are constrained for the substrate graphene (see the insets in Fig. 1b). We plot the IED as

a function of relative displacement along y-axis, where interlayer energy density was normalized as $U_{\mathrm{N}} = [U(u_x, u_y, u_z) - U_0(u_z = 0)]/U_1(u_z = 0)$. Initially, the graphene film is in AA stacking order relative to the substrate, which corresponds to the minimum interlayer potential energy state. AB stacking switches to AA stacking in case of film gliding distance a and further switches to BA stacking with the film gliding distance $2a$. Due to geometrical symmetry, AB stacking and BA stacking corresponds to the same potential energy state. For simplicity, we name the two modes both as AB stacking. Note that the interlayer potential energy of Saddle Point (SP) stacking is larger than AB stacking but far less than AA stacking.

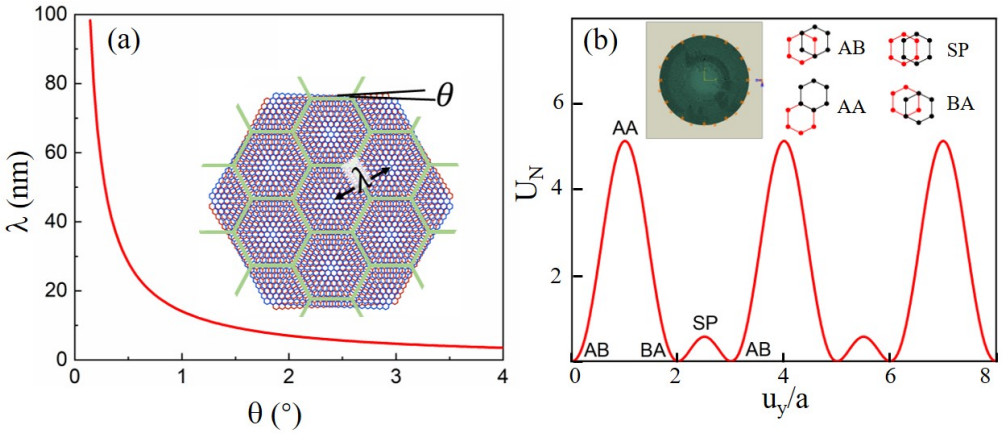

Figure 1. (a) Schematic of Moiré Pattern and its periode λ function of the twist angle for TBG films (as inset, an example is depicted); (b) interlayer potential energy density is depicted as a function of relative displacements u_y/a.

The TBG demonstrates extraordinary physical properties, i.e., insulator behavior and superconductivity, mainly at its initial twisted stage [15,16,32]. Therefore, we focus on the deformation behavior of the TBG with small twist angles. In Fig. 2 we show at different twist angles the out-of-plane displacement u_z, IED, Strain energy density (SED), distortion energy density (DED) and effective shear strain ε_i. It is observed that AA stacked domains first appear in the edges and gradually evolves to the inner domain. The distribution of out-of-plane displacement u_z agrees well with those of IED, corresponding to maximum interlayer potential energy state. The stripes that connect different AA stacked domains are SP stacked domains. Amplitudes of u_z and IED are invariant with the increment of twist angles, as shown in Fig. 3. By contrast, shear strain and SED in SP stacked domains decrease gradually as the twist angle increases. Indeed, the maximum strain is about 0.1% as the twist angle reaches 2°, demonstrating that the strain energy is negligible and the twisting behavior tends to be a rigid one. Besides, the in-plane strain disappears when the twist angle reaches 60°, indicating that the film relative to the substrate recovers to AB stacking order. We should note that the deformation and strain are significant in case of small twist angles (smaller than 2°), which will result in structural variations of the lattices and further lead to different physical properties.

We define quantitatively the AA (SP) stacked domain in Fig. 4, and plot the geometrical diameters as functions of the twist angle. For rigid twisting, we have

$$d_{\mathrm{AA}} = \frac{a}{\theta}, w_{\mathrm{SP}} = \frac{a}{2\theta}. \tag{2.2}$$

It is observed in Fig. 4 that the deformations have few influences on the Moiré pattern diameter λ, but significantly reduces the AA stacking diameter and SP stacking width, especially at small-twist-angles. Besides, local AB stacked domain turns around by a small angle, which is indicated by the difference between the dotted line and red points in Fig. 4e. Generally, AA stacking point

is not affected by the deformations, and can be modeled as rigid rotation during the bilayer graphene twisting process. We define a triangular unit cell characterized by three AA stacking points and show the variations of AA/AB/SP stacking domains within each unit cell in Fig. 4f. With the increment of twist angles, SP (AB) stacking domains increase (decrease) linearly until the twist angle reaches around 0.75°, then both the SP and AB stacking domains decrease by a rate far less than their initial variation rates. AA stacking domain increases with the twist angles, but the increasing rate drops a bit when the twist angle goes beyond 0.75°.

3. Theoretical analysis on deformation characteristics of twisted bilayer graphene

(a) Rigid twisting behavior of the graphene film

For a rigid twisted graphene film with constrained normal displacement u_z, the relative displacement field can be expressed as

$$\begin{cases} u_x = r[\cos(\theta_0+\theta)-\cos(\theta_0)] \\ u_y = r[\sin(\theta_0+\theta)-\sin(\theta_0)], \\ u_z = 0 \end{cases} . \tag{3.1}$$

where $\theta_0(\theta)$ is the angle between x-axis and the direction of the point before (after) twisting, as shown in Fig. 5a. The mean IED can be expressed as

$$U_{\mathrm{I_{ave}}} = \frac{\int_0^R \int_0^{2\pi} U(u_x,u_y,u_z) r dr d\theta_0}{\pi R^2}, \tag{3.2}$$

where R is the radius of the graphene film and $U(u_x,u_y,u_z)$ is the interlayer potential energy (per unit area) determined by [34,35]

$$U(u_x,u_y,u_z) = U_0(U_z) + U_1(U_z) f(u_x,u_y). \tag{3.3}$$

On the right-hand side of Eq. (3.3), the first term describes the dependence of the interaction potential energy on the normal separation u_z in a commensurate AB stacking order $u_x = u_y = 0$ and takes the form [36]

$$U_0(U_z) = \frac{\varepsilon_0}{A_0}\left[-\frac{5}{3}\left(\frac{z_0}{z_0+u_z}\right)^4 + \frac{2}{3}\left(\frac{z_0}{z_0+u_z}\right)^{10}\right]. \tag{3.4}$$

where $z_0 = 0.334$ nm is the equilibrium separation, $\varepsilon_0 = 0.0411$ eV, $A_0 = \frac{3\sqrt{3}}{4}a^2$ with $a = 0.142$ nm denotes the carbon-carbon bond length in the graphene. The adhesion energy for the commensurate AB stacking order is thus obtained as $\varepsilon_0/A_0 = 0.25\ \mathrm{J/m^2}$. The second term on the right-hand side quantifies the periodic corrugation of the potential energy with respect to in-plane displacements u_x and u_y, from the commensurate stacking with

$$f(u_x,u_y) = \frac{3}{2} + \cos(G_1(u_y-a)) + 2\cos\left(\frac{G_1(u_y-a)}{2}\right)\cos\left(\frac{\sqrt{3}G_1 u_x}{2}\right), \tag{3.5}$$

and

$$U_1(U_z) = \frac{\varepsilon_1}{A_0}\left[-\left(\frac{z_0}{z_0+u_z}\right)^4 + \beta\left(\frac{z_0}{z_0+u_z}\right)^{10}\right]. \tag{3.6}$$

where $G_1 = 1.33\pi/a$, $\varepsilon_1 = 1.33\times10^{-4}$ eV, $\beta = 28.7$; the values of ε_1 and β are obtained by fitting to atomistic calculations [37].

The mean IED value $U_{I_{ave}}$ increases gradually to its maximum value as the twist angle reaches the critical value θ_{cr}, as shown in Fig. 5b. Note that initially the graphene film is in AB stacking order relative to the substrate, and corresponding IED is $\varepsilon_0/A_0 = 0.25\mathrm{J/m^2}$. Here we define the

state when the film is completely stripped from the substrate as zero point of the potential energy density. After the twist angle reaches its critical value, the mean value $U_{\mathrm{I_{ave}}}$ decreases gradually to its minimum value and then fluctuates around a constant value $-U_0(u_z=0)+U_1(u_z=0)f(u_x=u_y=0)$. Besides, the oscillation period is reversely related to the film radius. In Fig. 5 we plot the critical twist angle θ_{cr} and first oscillation period θ_λ as functions of the radius of the graphene film disk.

Now we turn to analyze the underlying mechanism that results in the oscillation behavior. We study the unit cell shown in Fig. 6a and find that the relative displacement field meets following constraint:

$$\int_{\frac{-\sqrt{3}\lambda}{6}}^{\frac{\sqrt{3}\lambda}{3}}\int_{\frac{\sqrt{3}}{3}(x-\frac{\sqrt{3}\lambda}{3})}^{\frac{\sqrt{3}}{3}(\frac{\sqrt{3}\lambda}{3}-x)}\left[f(u_x,u_y)-\frac{3}{2}\right]dydx=0. \tag{3.7}$$

If we fix the out-of-plane displacements during the twisting process as $u_z=c$, we can obtain following relationship for any twist angle θ:

$$\frac{\int_{\frac{-\sqrt{3}\lambda}{6}}^{\frac{\sqrt{3}\lambda}{3}}\int_{\frac{\sqrt{3}}{3}(x-\frac{\sqrt{3}\lambda}{3})}^{\frac{\sqrt{3}}{3}(\frac{\sqrt{3}\lambda}{3}-x)}U(u_x(\theta),u_y(\theta))dydx}{A_0}=U_0(c)+\frac{3}{2}U_1(c). \tag{3.8}$$

where the Moiré pattern diameter is $\lambda=\sqrt{3}a/\sqrt{2(1-\cos(\theta))}$, the unit cell area is $A_0=\frac{\sqrt{3}}{4}\lambda^2$ denotes interlayer potential energy and the in-plane displacements are expressed by

$$\begin{cases} u_x(\theta)=\sqrt{x^2+y^2}\left[\cos(\tan^{-1}(\frac{y}{x})+\theta)-\cos(\tan^{-1}(\frac{y}{x}))\right] \\ u_y(\theta)=\sqrt{x^2+y^2}\left[\sin(\tan^{-1}(\frac{y}{x})+\theta)-\sin(\tan^{-1}(\frac{y}{x}))\right]. \end{cases} \tag{3.9}$$

We observe from Eq. (3.9) that the mean interlayer potential energy of a unit cell is invariant with the twist angle, indicating that the oscillation behavior is induced by edge effects. In the initial twisting stage of the graphene film, the deformations result in a drop of interlayer potential energy and a rise of strain energy, which makes the total energy smaller than that of the rigid counterpart. As the strain increases, the strain energy gradually decreases, and the total energy difference between the deformed twisting behavior and rigid twisting behavior was reduced correspondingly.

(b) Deformable twisting behavior of the graphene film

We show in Fig. 7 the Interlayer potential energy density of a graphene in rigid twisting ($\mathrm{IED_r}$) and in deformable twisting ($\mathrm{IED_d}$) and the difference between the two terms (Δ_{IED}), in case of the twist angle $\theta=0.6^\circ$ and the displacement $u_z=0$. It is observed that in-plane deformations have significant influences on the IED of AA stacked domains, but have few influences on AB stacked domains and SP stacked domains. Besides, in-plane deformations (shear deformations) mainly exist in SP stacked domains. The film strain distributes uniformly in SP stacked domains with quasi-rectangular shapes, which denotes that displacements of contrary directions are generated on the edges of such quasi-rectangular shapes and results in uniformly distributed shear strain. Note that the IED of SP stacked domains are less than that of AA stacked domains. Then we can describe the deformation behavior in following ways: we first conduct rigid twisting by a twist angle θ, then releases the rigid constraints; AA stacked domains continue to twist in the same direction by an angle α while AB stacked domains twist in the opposite direction by an angle β.

The work done by AB stacked domains to overcome the interlayer reactions is expressed by

$$W_{\mathrm{AB}}(\theta)=\int_{\frac{-\sqrt{3}\lambda}{12}}^{\frac{\sqrt{3}\lambda}{6}}\int_{\frac{\sqrt{3}}{3}(x-\frac{\sqrt{3}\lambda}{6})}^{\frac{\sqrt{3}}{3}(\frac{\sqrt{3}\lambda}{6}-x)}\left[U(u_x(\theta),u_y(\theta))-U(u_x=u_y=0)\right]dydx\approx\frac{U_1\lambda^2}{5}. \tag{3.10}$$

Similarly, the work done by AB stacked domains to turn back by an angle β is expressed by

$$W_{\mathrm{AB}}(\theta-\beta)=\int_{-\frac{\sqrt{3}\lambda}{12}}^{\frac{\sqrt{3}\lambda}{6}}\int_{\frac{\sqrt{3}}{3}(x-\frac{\sqrt{3}\lambda}{6})}^{\frac{\sqrt{3}}{3}(\frac{\sqrt{3}\lambda}{6}-x)}\left[U(u_x(\theta-\beta),u_y(\theta-\beta))-U(u_x=u_y=0)\right]dydx. \tag{3.11}$$

The work can be approximated by

$$W_{\mathrm{AB}}(\theta-\beta)\approx\frac{U_1\lambda^2}{5}(k^2-2k+1). \tag{3.12}$$

where $k=1-\beta/\theta$, $U_1(u_z)=(\beta-1)\varepsilon_1/A_0$, $\lambda=\sqrt{3}a/\sqrt{2(1-\cos(\theta))}$. In the interval $k\in[0,1]$ the approximated solution and accurate solution from Eq. (3.11) show good agreement, as depicted in Fig. 8a.

As mentioned before, the film deformation are mainly shear deformations existing in the SP stacked domains, as shown in Fig. 7d. We can obtain the shear strain of a unit cell as

$$W_{\mathrm{S}}=3t(\lambda-2R_{\mathrm{A}})w_{\mathrm{P}}\frac{G\gamma^2}{2}. \tag{3.13}$$

where the coefficient "3" is applied due to the fact that three SP stacked domains exist in each unit cell, t is the film thickness, G is the shear modulus, w_P is half-width of SP stacked domains, γ is the shear strain energy of SP stacked domains determined by

$$\gamma=\frac{\partial u_y}{\partial x}+\frac{\partial u_x}{\partial y}=\beta+\alpha\frac{\frac{\sqrt{3}}{2}r}{\frac{\lambda}{2}-\frac{\sqrt{3}}{2}r}=\alpha\left(\frac{\theta}{\theta+2\alpha}+1\right). \tag{3.14}$$

Note that film strain energy in AB stacked domains is far less than that in SP stacked domains. Therefore, we safely ignore the deformations in AB stacked domains and view them as rigid twisting. From geometrical compatibility, we have

$$\frac{\frac{a}{2}}{\sin(\theta+\alpha)}\alpha=\frac{\frac{a}{2}}{\sin(\theta-\alpha)}\beta. \tag{3.15}$$

As α and β are small, Eq. (3.15) can be simplified as

$$\beta=\frac{\theta\alpha}{\theta+2\alpha}. \tag{3.16}$$

Then we have

$$W_{\mathrm{P}}=\frac{a}{4\sin(\theta+\beta)}\approx\frac{a}{4(\theta+\beta)}; \tag{3.17}$$

$$R_{\mathrm{A}}=\frac{a}{2\sin(\theta+\alpha)}\approx\frac{a}{2(\theta+\alpha)}. \tag{3.18}$$

Substituting Eqs. (3.14) (3.18) into Eq. (3.13), we can express the shear strain energy of a unit cell as

$$W_{\mathrm{S}}=\frac{3Gta}{8}\left(\lambda-\frac{a}{\theta+\alpha}\right)\frac{(\theta+2\alpha)\alpha^2}{\theta^2+3\theta\alpha}\left(\frac{\theta}{\theta+2\alpha}+1\right)^2. \tag{3.19}$$

Now we turn to the interlayer potential energy of AA stacked domains. For a graphene film/substrate system in AA stacking order, the interlayer potential energy is

$$U_{\mathrm{AA}}=U_0+U_1\left[\frac{3}{2}+\cos(G_1u_y)+2\cos\left(\frac{G_1u_y}{2}\right)\cos\left(\frac{\sqrt{3}G_1u_x}{2}\right)\right], \tag{3.20}$$

The work needed to twist a graphene film disk by an angle θ is expressed as

$$W_\theta=\int_0^r\int_{-\sqrt{r^2-x^2}}^{\sqrt{r^2-x^2}}\left[U_{\mathrm{AA}}(u_x(\theta),u_y(\theta))-U_{\mathrm{AA}}(u_x=u_y=0)\right]dydx\approx-\frac{\sqrt{3}+1}{2}U_1\pi\left(\frac{a}{2\theta}\right)^2. \tag{3.21}$$

If we increase the twist angle to $\theta+\alpha$, the stored energy becomes

$$W_{\theta+\alpha}=\int_0^r\int_{-\sqrt{r^2-x^2}}^{\sqrt{r^2-x^2}}\left[U_{\mathrm{AA}}(u_x(\theta+\alpha),u_y(\theta+\alpha))-U_{\mathrm{AA}}(u_x=u_y=0)\right]dydx, \tag{3.22}$$

which can be approximated by

$$W_{\theta+\alpha}\approx\frac{\sqrt{3}+1}{2}U_1\pi\left(\frac{a}{2\theta}\right)^2\left(\frac{\sqrt{3}+1}{4}\frac{\alpha^2}{\theta^2}-\frac{2\alpha}{\theta}-1\right). \tag{3.23}$$

In the case $\alpha/\theta<2$, the approximated solution and accurate solution from Eq. (3.22) are in good agreement, as shown in Fig. 8b. For the studied unit cell, the total energy variations induced by film deformations can be obtained by

$$U_{\mathrm{relaxed}}=W_{\mathrm{S}}+\left(W_{\mathrm{AB}}(\theta-\beta)-W_{\mathrm{AB}}(\theta)\right)+\frac{1}{2}\left(W_{\theta+\alpha}-W_{\theta}\right). \tag{3.24}$$

Combining Eq. (3.8), we obtain the total energy of a unit cell of the twisted graphene film as $U_{\mathrm{relaxed}}+U_0+3U_1/2$. Using minimum energy principle, we get

$$\frac{\partial}{\partial\alpha}\left(U_{\mathrm{relaxed}}+U_0+3U_1/2\right)=0. \tag{3.25}$$

Substituting Eqs. (3.4) (3.6) (3.24) into Eq. (3.25), we can obtain the relation between α and θ as

$$\begin{aligned}&\frac{3Gta}{8}\left(\lambda+\frac{a}{(\theta+\alpha)^2}\right)\frac{(\theta+2\alpha)\alpha^2}{\theta^2+3\theta\alpha}\left(\frac{\theta}{\theta+2\alpha}+1\right)^2\\&+\frac{U_1\lambda^2}{5}\frac{2\beta}{\theta^2}\frac{\theta^2}{(\theta+2\alpha)^2}+\frac{3Gta}{8}\left(\lambda-\frac{a}{\theta+\alpha}\right)\frac{2\alpha\theta^3+9\alpha^2\theta^2+12\alpha^3\theta}{(\theta^2+3\alpha\theta)^2}2\alpha\left(\frac{\theta}{\theta+2\alpha}+1\right)^2\\&-\frac{3Gta}{8}\left(\lambda-\frac{a}{\theta+\alpha}\right)\frac{(\theta+2\alpha)\alpha^2}{\theta^2+3\alpha\theta}2\left(\frac{\theta}{\theta+2\alpha}+1\right)\frac{2\theta}{(\theta+2\alpha)^2}-\frac{\sqrt{3}+1}{4}U_1\pi\left(\frac{a}{2\theta}\right)^2\left(\frac{2}{\theta}-\frac{\sqrt{3}+1}{2}\frac{\alpha}{\theta^2}\right)=0\end{aligned} \tag{3.26}$$

Given a twist angle θ, we can obtain the additional twist angle α of AA stacked domains from Eq. (3.26), and further get the additional twist angle β of AB stacked domains from Eq. (3.15), and finally obtain SP stacked domain width w_P and AA stacked domain radius R_A from Eq. (3.17) and Eq. (3.18), respectively. We observe in Fig. 9a the relation $\alpha/\theta<1.5,\beta/\theta<0.5$ during the small-angle-twisting process, indicating that the approximated solutions from Eq. (3.12) and Eq. (3.23) are valid. Besides, the theoretical predictions agree well with the finite element analysis when the twist angle reaches 0.75°, demonstrating the accuracy of our proposed analytical model. When the twist angle is beyond 2°, the influences of graphene film deformations can be neglected and the bilayer graphene can be viewed as rigid twisting. However, we notice some differences between theoretical results and simulations when the twist angle is very small. This difference may imply different deformation mechanism, which will be our further consideration.

4. Conclusion

The torsional deformation behavior and strain localization of TBG has been studied numerically and analytically. It is found that the periodicity and symmetry of interlayer van der Waals force makes the mean strain energy density invariant during the rigid twisting process. Both in-plane and out-of-plane deformations are observed after releasing the rigid twisting constraints, due to the strong coupling of in-plane and out-of-plane displacements. Out-of-plane deformations agree well with the IED distributions, and have invariant amplitudes with increasing twist angles. Compared with rigid twisting, the in-plane deformations are mainly observed in the inner domain of the unit cells, while the shapes and sizes of the edges are invariant. Following this phenomenon, we derived the total strain potential energy function of the deformable system, and further obtained the film deformations as functions of the twist angles. Results show that the shear strain distributes uniformly in SP stacked domains and decreases sharply with the increment of twist angles. The influences of graphene film deformations is significant when the twist angle is less than 2°.

Data Accessibility. This article does not contain any additional data.

Authors' Contributions. Q.X.J: Formal analysis, Writing original draft, Investigation and Project administration. Z.M.X.: Conceptualization, Formal analysis, Editing. Z.X.Z: Formal analysis. Z.B.C.: Methodology, Data curation. M.K.: Supervision, Validation, Review and editing. C.G.W.: Supervision, Validation, Project administration, Review and editing.

Competing Interests. We declare we have no competing interests.

Funding. This work was supported by the National Natural Science foundation of China [grant numbers 12172102, 11872160].

Acknowledgements. Z.M.X. thanks Dr. Rui Huang at the University of Texas at Austin for many valuable discussions.

References

1. S. Kumar, D. M. Parks, On the hyperelastic softening and elastic instabilities in graphene, Proceedings of the Royal Society A: Mathematical, Physical and Engineering Sciences 471 (2173) (2015) 20140567.
2. Y. Wang, Y. Zhu, F. Wang, X. Liu, H. Wu, Super-elasticity and deformation mechanism of three-dimensional pillared graphene network structures, Carbon 118 (2017) 588–596.
3. H. Wu, X. Liu, Tuning electromechanics of dynamic ripple pattern in graphene monolayer, Carbon 98 (2016) 510–518.
4. H. Zhong, J. Xia, F. Wang, H. Chen, H. Wu, S. Lin, Graphene-piezoelectric material heterostructure for harvesting energy from water flow, Advanced Functional Materials 27 (5) (2017) 1604226.
5. Q. Li, K.-S. Kim, Micromechanics of friction: effects of nanometre-scale roughness, Proceedings of the Royal Society A: Mathematical, Physical and Engineering Sciences 464 (2093) (2008) 1319–1343.
6. X. Zheng, L. Gao, Q. Yao, Q. Li, M. Zhang, X. Xie, S. Qiao, G. Wang, T. Ma, Z. Di, et al., Robust ultra-low-friction state of graphene via moiré superlattice confinement, Nature communications 7 (1) (2016) 1–7.
7. X.-Y. Sun, H. Hu, C. Cao, Y.-J. Xu, Anisotropic vacancy-defect-induced fracture strength loss of graphene, RSC Advances 5 (18) (2015) 13623–13627.
8. K. J. Ooi, D. T. Tan, Nonlinear graphene plasmonics, Proceedings of the Royal Society A: Mathematical, Physical and Engineering Sciences 473 (2206) (2017) 20170433.
9. T. L. Zinenko, A. Matsushima, A. I. Nosich, Terahertz range resonances of metasurface formed by double-layer grating of microsize graphene strips inside dielectric slab, Proceedings of the Royal Society A 476 (2240) (2020) 20200173.
10. M. Farhat, S. Guenneau, H. Bağcı, Exciting graphene surface plasmon polaritons through light and sound interplay, Physical review letters 111 (23) (2013) 237404.
11. R. Alaee, M. Farhat, C. Rockstuhl, F. Lederer, A perfect absorber made of a graphene micro-ribbon metamaterial, Optics express 20 (27) (2012) 28017–28024.
12. M. Amin, M. Farhat, H. Bağcı, An ultra-broadband multilayered graphene absorber, Optics express 21 (24) (2013) 29938–29948.
13. J. Christensen, A. Manjavacas, S. Thongrattanasiri, F. H. Koppens, F. J. García de Abajo, Graphene plasmon waveguiding and hybridization in individual and paired nanoribbons, ACS nano 6 (1) (2012) 431–440.
14. E. Y. Andrei, A. H. MacDonald, Graphene bilayers with a twist, Nature materials 19 (12) (2020) 1265–1275.
15. Y. Cao, V. Fatemi, S. Fang, K. Watanabe, T. Taniguchi, E. Kaxiras, P. Jarillo-Herrero, Unconventional superconductivity in magic-angle graphene superlattices, Nature 556 (7699) (2018) 43–50.
16. Y. Cao, V. Fatemi, A. Demir, S. Fang, S. L. Tomarken, J. Y. Luo, J. D. Sanchez-Yamagishi, K. Watanabe, T. Taniguchi, E. Kaxiras, et al., Correlated insulator behaviour at half-filling in magic-angle graphene superlattices, Nature 556 (7699) (2018) 80–84.
17. S. Zhang, A. Song, L. Chen, C. Jiang, C. Chen, L. Gao, Y. Hou, L. Liu, T. Ma, H. Wang, et al., Abnormal conductivity in low-angle twisted bilayer graphene, Science advances 6 (47) (2020) eabc5555.

18. A. Nimbalkar, H. Kim, Opportunities and challenges in twisted bilayer graphene: a review, Nano-Micro Letters 12 (1) (2020) 1–20.
19. Y. Cao, D. Rodan-Legrain, O. Rubies-Bigorda, J. M. Park, K. Watanabe, T. Taniguchi, P. Jarillo-Herrero, Tunable correlated states and spin-polarized phases in twisted bilayer–bilayer graphene, Nature 583 (7815) (2020) 215–220.
20. J. L. Dos Santos, N. Peres, A. C. Neto, Graphene bilayer with a twist: electronic structure, Physical review letters 99 (25) (2007) 256802.
21. J. Christensen, M. Kadic, O. Kraft, M. Wegener, Vibrant times for mechanical metamaterials, Mrs Communications 5 (3) (2015) 453–462.
22. M. Kadic, R. Schittny, T. Bückmann, C. Kern, M. Wegener, Hall-effect sign-inversion in a realizable 3d metamaterial, Phys. Rev. X 5 (2015) 021030.
23. C. Kern, M. Kadic, M. Wegener, Experimental evidence for sign reversal of the hall coefficient in three-dimensional metamaterials, Phys. Rev. Lett. 118 (2017) 016601.
24. X. Chen, Q. Ji, J. Wei, H. Tan, J. Yu, P. Zhang, V. Laude, M. Kadic, Light-weight shell-lattice metamaterials for mechanical shock absorption, International Journal of Mechanical Sciences 169 (2020) 105288.
25. M. Kadic, G. W. Milton, M. van Hecke, M. Wegener, 3d metamaterials, Nature Reviews Physics 1 (3) (2019) 198–210.
26. Y. Chen, M. Kadic, S. Guenneau, M. Wegener, Isotropic chiral acoustic phonons in 3d quasicrystalline metamaterials, Physical Review Letters 124 (23) (2020) 235502.
27. Y. Chen, M. Kadic, M. Wegener, Roton-like acoustical dispersion relations in 3d metamaterials, Nature communications 12 (1) (2021) 1–8.
28. J. A. Iglesias Martínez, M. F. Groß, Y. Chen, T. Frenzel, V. Laude, M. Kadic, M. Wegener, Experimental observation of roton-like dispersion relations in metamaterials, Science advances 7 (49) (2021) eabm2189.
29. K. Wang, Y. Chen, M. Kadic, C. Wang, M. Wegener, Nonlocal interaction engineering of 2d roton-like dispersion relations in acoustic and mechanical metamaterials, Communications Materials 3 (1) (2022) 1–11.
30. J. S. Alden, A. W. Tsen, P. Y. Huang, R. Hovden, L. Brown, J. Park, D. A. Muller, P. L. McEuen, Strain solitons and topological defects in bilayer graphene, Proceedings of the National Academy of Sciences 110 (28) (2013) 11256–11260.
31. K. Zhang, E. B. Tadmor, Structural and electron diffraction scaling of twisted graphene bilayers, Journal of the Mechanics and Physics of Solids 112 (2018) 225–238.
32. N. P. Kazmierczak, M. Van Winkle, C. Ophus, K. C. Bustillo, S. Carr, H. G. Brown, J. Ciston, T. Taniguchi, K. Watanabe, D. K. Bediako, Strain fields in twisted bilayer graphene, Nature materials 20 (7) (2021) 956–963.
33. K. Hermann, Periodic overlayers and moiré patterns: theoretical studies of geometric properties, Journal of Physics: Condensed Matter 24 (31) (2012) 314210.
34. H. Kumar, D. Er, L. Dong, J. Li, V. B. Shenoy, Elastic deformations in 2d van der waals heterostructures and their impact on optoelectronic properties: predictions from a multiscale computational approach, Scientific reports 5 (1) (2015) 1–11.
35. H. Kumar, L. Dong, V. B. Shenoy, Limits of coherency and strain transfer in flexible 2d van der waals heterostructures: formation of strain solitons and interlayer debonding, Scientific reports 6 (1) (2016) 1–8.
36. K. Zhang, E. B. Tadmor, Energy and moiré patterns in 2d bilayers in translation and rotation: A study using an efficient discrete–continuum interlayer potential, Extreme Mechanics Letters 14 (2017) 16–22.
37. Z. Xue, G. Chen, C. Wang, R. Huang, Peeling and sliding of graphene nanoribbons with periodic van der waals interactions, Journal of the Mechanics and Physics of Solids 158 (2022) 104698.

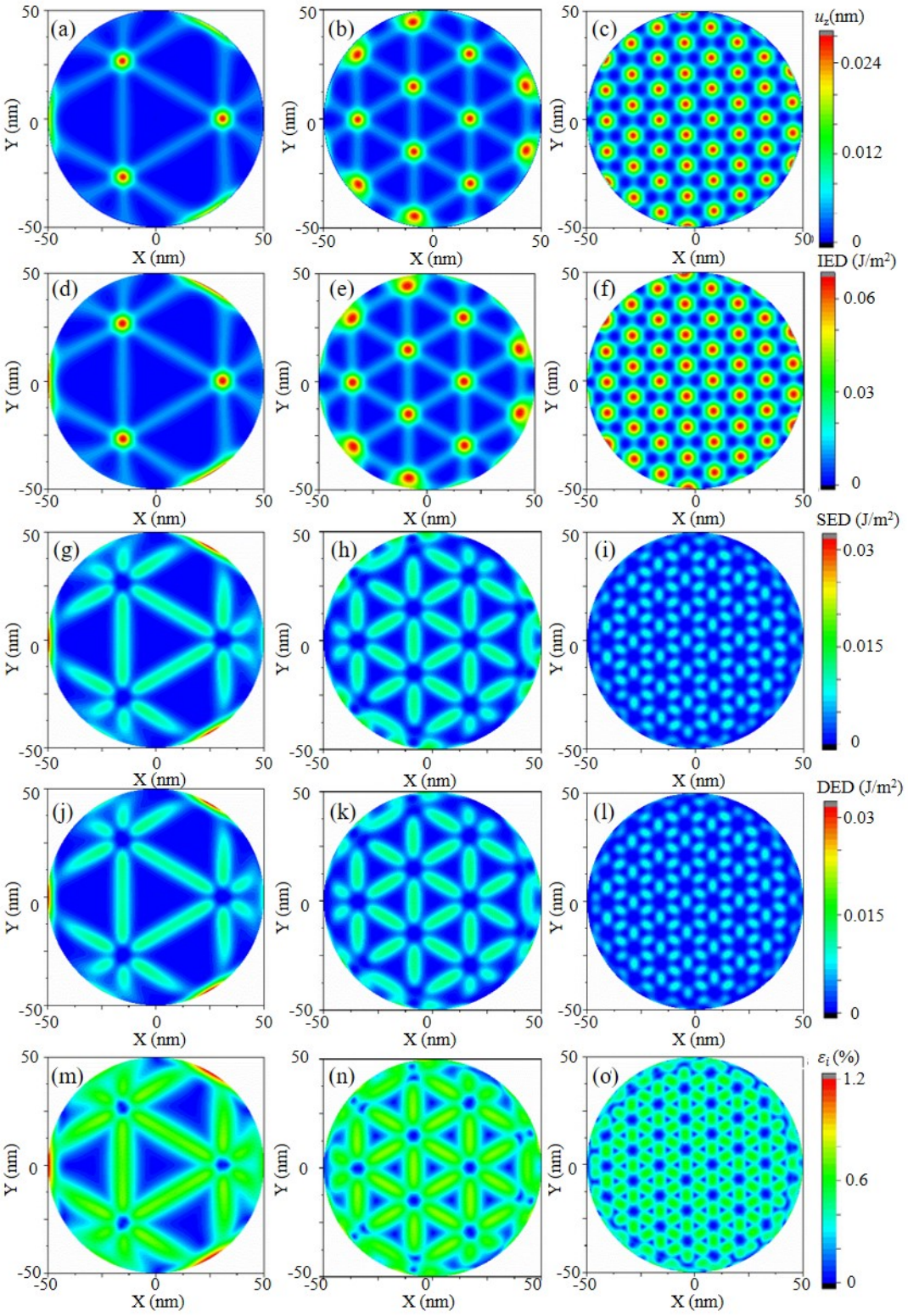

Figure 2. (a, b, c) Out-of-plane displacements component u_z, (d, e, f) IED, (g, h, i) SED, (j, k, l) DED, and (m, n, o) equivalent strain distribution at different twist angles 0.3°, 0.5°, and 1°, respectively.

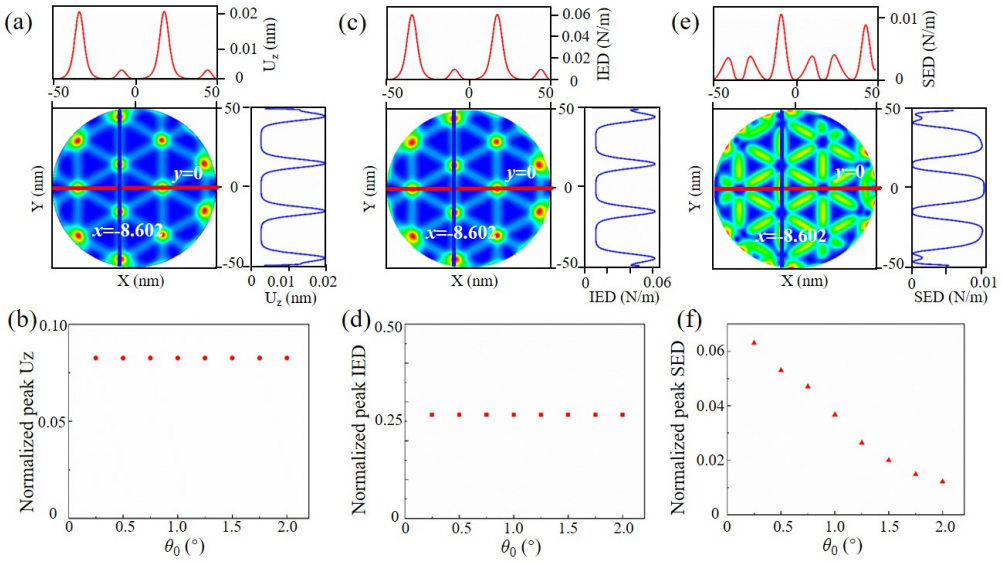

Figure 3. (a) The out-of-plane displacement u_z, (c) IED, and (e) the distribution of SED as the twist angle $\theta = 0.5°$; (b, d, f) the corresponding maximum value as functions of the twist angle.

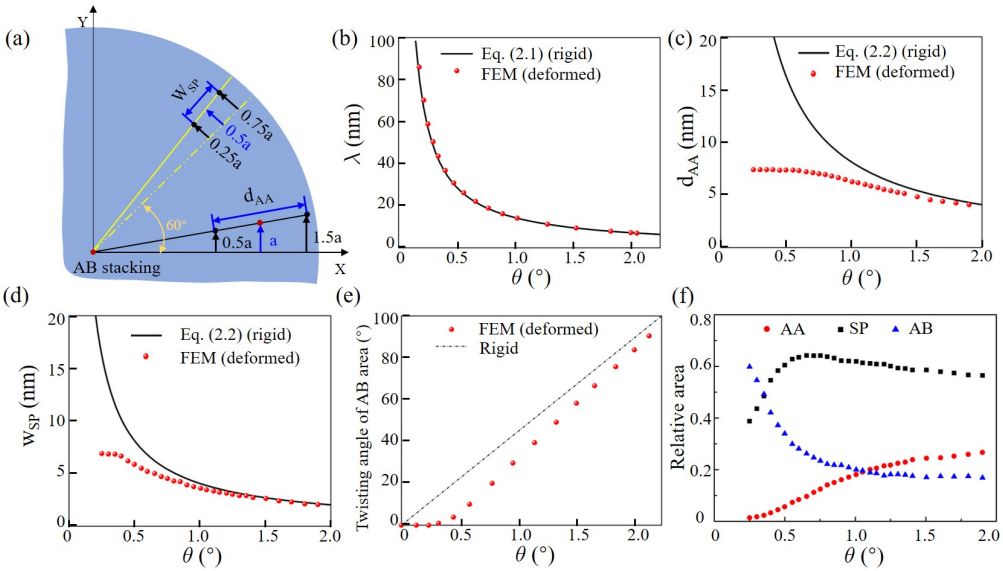

Figure 4. (a) Schematic of different stacking domains; functions of the twist angle for: (b) the size of moiré pattern, (c) the AA stacking diameter, (d) the width of SP stacking, (e) the twist angle of AB stacking and (f) relative stacking order domains.

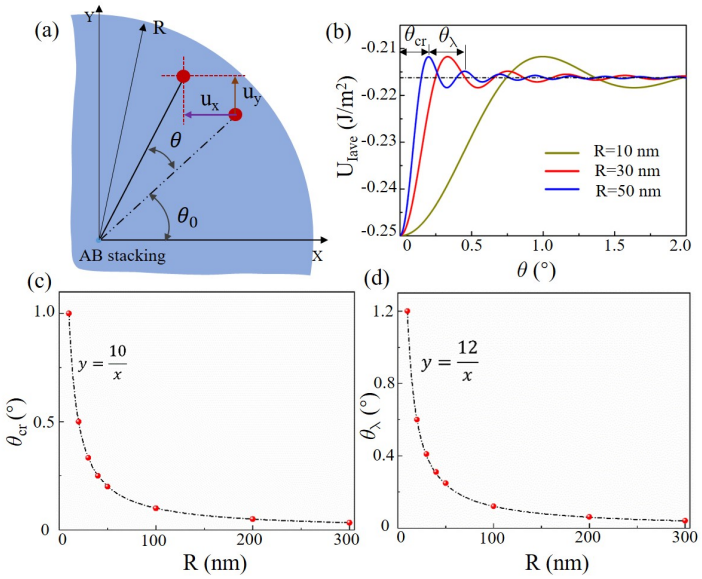

Figure 5. (a) Schematic of relative displacements; (b) the IED as a function of twist angles; (c) the critical twist angle and (d) the first oscillation period as functions of the graphene disk diameter.

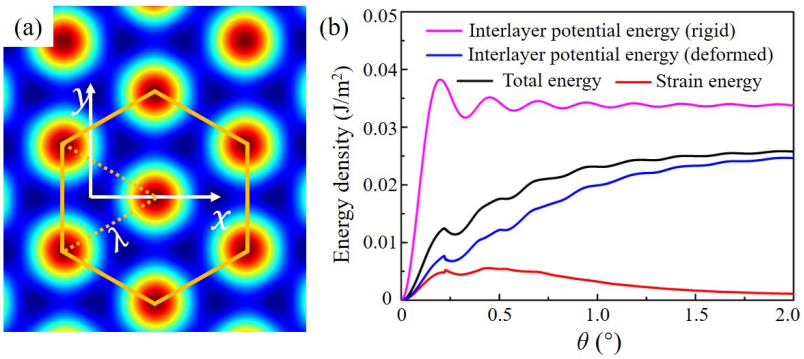

Figure 6. (a) Contour of the IED for rigid twisting bilayer graphene; (b) the energy densities as a function of twist angles for a graphene disk with diameter of 50 nm.

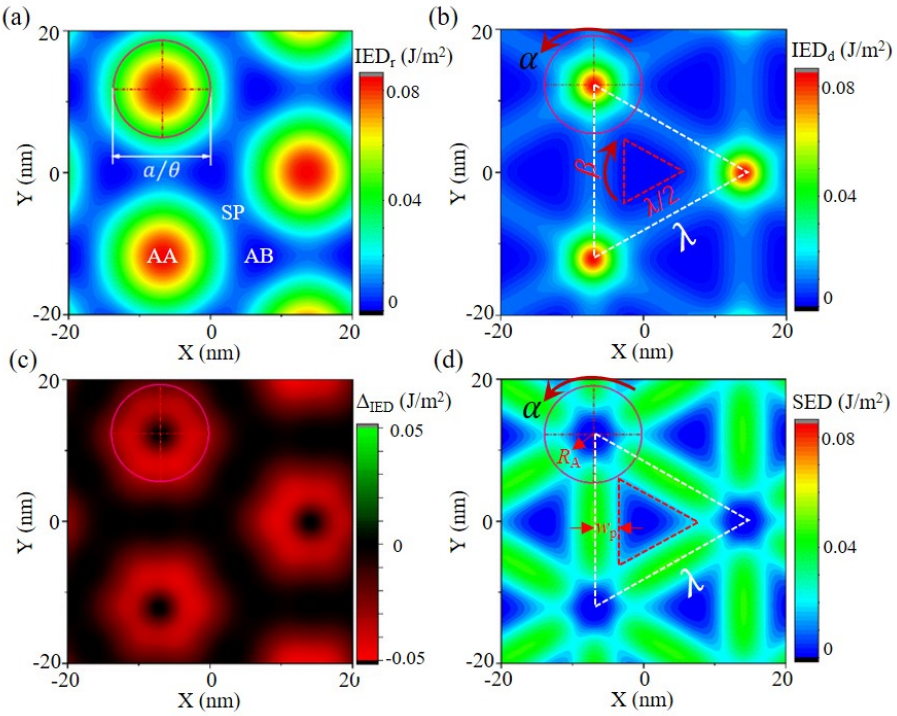

Figure 7. The IED of (a) rigid twisting and (b) deformable twisting; (c) the difference of IED between rigid and deformable twisting; (d) SED of the graphene film. All the results are considered for the twist angle $\theta = 0.6^\circ$ and the displacement $u_z = 0$.

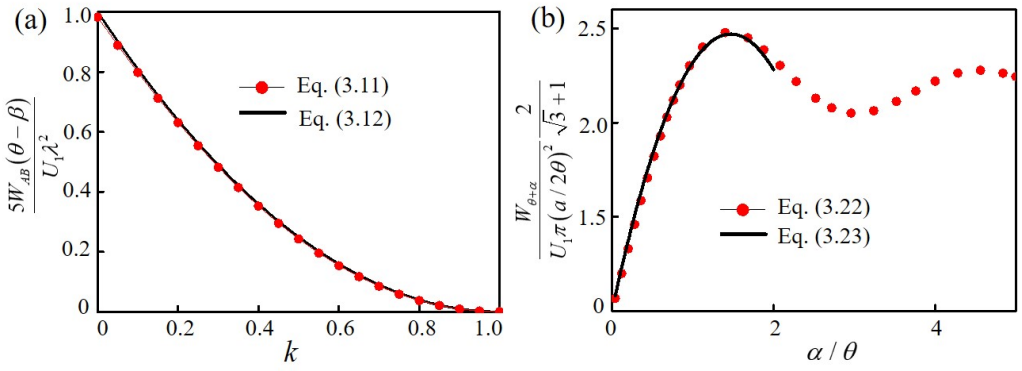

Figure 8. The interlayer potential energy of (a) AB stacked domain and (b) AA stacked domain as functions of additional twist angles.

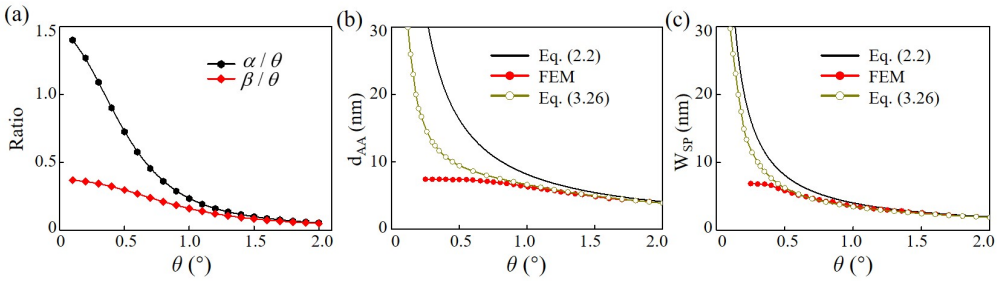

Figure 9. (a) The additional twist angles of AA and AB stacking area, (b) dimeter of AA stacking area, (c) width of SP stacking area as functions of twist angle θ.